

An improved geometric solution for WFPC2

Stefano Casertano and Michael S. Wiggs
October 29, 2001

ABSTRACT

We present an improved solution for the geometric distortion in WFPC2, based on multiple observations of a rich stellar field. We also quantify the long-term variation of the relative position of the detectors by tracking the position of the K spots over time. We suggest possible avenues to develop an improved wavelength- and time-dependent geometric solution for WFPC2.

Introduction and history

The combination of the Optical Telescope Assembly (OTA) and of the WFPC2 internal optics produces a systematic geometric distortion in the images observed with WFPC2. The mapping between image pixels and a standard two-dimensional local representation of the sky, such as the tangent plane projection, is not a simple rigid transformation of coordinates; detector pixels are not equally spaced on straight, perpendicular lines. A “geometric solution” for WFPC2 is a mapping between image pixels and sky position that can be used to reconstruct the relative positions of different image pixels in the sky. Such mappings are used to transform pixel coordinates into sky coordinates, such as by the STSDAS task **metric**, or to obtain rectified images, such as by the STSDAS tasks **wmosaic** and **drizzle**.

While geometric transformations are generally necessary for astronomical instruments, the case of WFPC2 is made more complex by the fact that the field of view is split into four areas, each of which is mapped onto a separate detector. The splitting is accomplished by a four-faceted mirror, the “pyramid.” Therefore four essentially separate geometric transformations are needed, one for each detector/pyramid facet. To make mat-

ters worse, the pyramid is in the aberrated beam, therefore the split of the field of view is not sharp; areas within 2'' of the pyramid edges will be actually mapped onto two (or more) separate detectors. Furthermore, the image of each facet does not completely fill each detector, therefore there is a border in each CCD which does not truly correspond to any point on the sky; those areas, "under" the pyramid so to speak, receive very little light from astronomical sources and are dark in uncalibrated images. Finally, there is evidence that the relative mapping of the four detectors onto the sky has been changing in time, most likely because of small changes in the physical position of the detectors themselves - therefore the mapping is a function of time.

The WFPC2 geometric distortion is generally defined by four transformations between each detector's (x,y) coordinates and a common rectilinear coordinate system, meant to coincide with tangent plane coordinates on the sky. Of course, the origin and orientation of this common coordinate system is arbitrary; we choose to reference it to the center of the Planetary Camera (PC), which is kept at the same position as in the previously published solutions by Holtzman et al (1995). For simplicity, the functional form of the transformation does not distinguish which areas of the detector are fully, partially, or not illuminated by the sky; care must be exercised when using the geometric transformation for pixels close to (or beyond) the pyramid edges.

Holtzman et al (1995), Gilmozzi et al (1995), and Trauger et al (1995) have produced descriptions of the WFPC2 geometric distortion that have been fruitfully used by WFPC2 observers over the years; we refer to these solutions as the Holtzman, Gilmozzi, and Trauger solutions, respectively. The Gilmozzi solution is expressed in terms of a combination of Legendre polynomials of third order - which includes terms of combined degree as high as 6 - and is based on multiple overlapping observations of the globular cluster NGC 1850, taken with both the WF/PC and the WFPC2 cameras. Holtzman used a complete third degree polynomial in x,y and derived his data from a series of substepped observations of a field in NGC 5198 (ω Cen). Trauger's solution used the same form as Holtzman, but the coefficients were allowed to be quadratic functions of the refraction index n of the MgF₂ field-flattener lenses; the solution in this case was derived from ray tracing through an optics model of the camera, and has fewer independent parameters than Holtzman's solution - i.e., several of the polynomial coefficients vanish or are identical by construction.

The Gilmozzi and Holtzman solutions are empirical, derived primarily from the internal consistency of WFPC2 (and WF/PC) observations. Their solutions optimize the consistency of the position of a large number of point sources when observed at different positions within the field of view. No prior knowledge of the positions of the point sources is required. Of course, this method cannot *completely* determine the geometric solution of the camera. For example, any overall scale factors must be determined from external considerations, since the same consistency can be obtained irrespective of the plate scale of the camera. In fact, any overall linear transformation of the geometric distortion will not

affect the consistency of the solution, and therefore drops out of the method. The Holtzman solution solves this indeterminacy by using the knowledge of the motions of the telescope between pointings, which were commanded to be on a grid with spacing of 16"; therefore the accuracy of the plate scale he determines corresponds to the accuracy of the small-angle motions of HST. The plate scale accuracy has been verified after the fact via measurements of the orbits of the moons of Uranus, compared with their computed ephemerides. Trauger limited his solutions to the quadratic and higher order terms, relying on the Holtzman solution for the main scale and orientation.

Observations and position measurements

The geometric distortion solution derived here uses multiple observations, at the same (or very similar) orientation, of a very rich star field in ω Cen obtained on June 13, 1997 for program CAL 6941. Observations were obtained in the filters F300W, F555W, and F814W; here we concentrate on the observations in F555W. Individual frames were obtained at each of 14 pointings, as follows:

1. a central pointing at RA 13 27 11.83, dec -47 29 54.7 (A in Figure 1), specified for the WFALL aperture
2. four pointings shifted by $\pm 35''$ in both x and y, forming a large X with the central pointing (B in Figure 1); the x and y directions refer to the corresponding pixel directions in the Planetary Camera
3. four pointings shifted by $\pm 15''$ in both x and y, forming a small X with the central pointing (C in Figure 1)
4. five pointings shifted by $+0.25''$ in x and y with respect to the pointings A and B in the large X (D in Figure 1).

The purpose of the large X is to ensure good overlap between the Wide Field Cameras, which are shifted by about half their size in each direction; the small X ensures good overlap between different pointings of the Planetary Camera. The D pointings help remove under-sampling effects for position measurements; their $0.25''$ shift corresponds to 2.5 pixels in the Wide Field Cameras and 5.5 pixels in the Planetary Camera. A complete list of the observations is given in Table 1.

Figure 1: Placement of image centers for Program 6941. The axes are aligned with the PC.

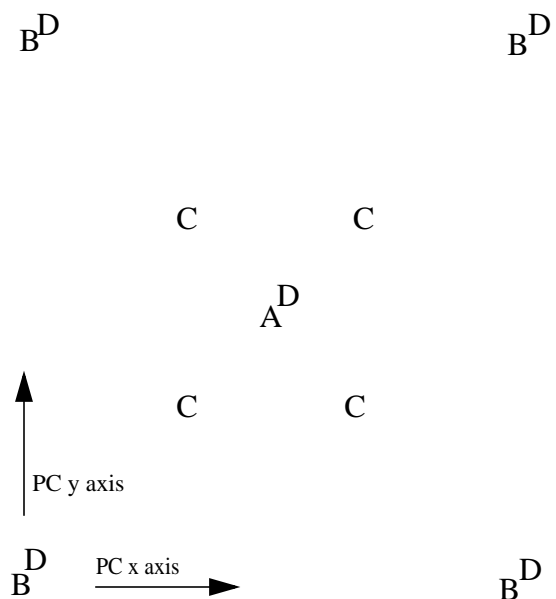


Table 1. Observations used in determining the June 1997 geometric solution

Dataset	Prog	RA	Dec	Filter	Exp.	Date	Start time (UT)
u40x010wmm	6941	13 27 13.53	-47 30 12.27	F555W	100.00	1997/06/13	1:37:14pm
u40x010xm	6941	13 27 14.51	-47 29 43.97	F555W	100.00	1997/06/13	1:43:14pm
u40x010ym	6941	13 27 11.72	-47 29 34.01	F555W	100.00	1997/06/13	1:49:14pm
u40x0101m	6941	13 27 12.62	-47 29 53.14	F300W	160.00	1997/06/13	8:23:14am
u40x0102m	6941	13 27 12.62	-47 29 53.14	F555W	100.00	1997/06/13	8:28:14am
u40x0103m	6941	13 27 12.62	-47 29 53.14	F814W	100.00	1997/06/13	8:32:14am
u40x0104m	6941	13 27 12.59	-47 29 53.29	F300W	160.00	1997/06/13	8:38:14am
u40x0105m	6941	13 27 12.59	-47 29 53.29	F555W	100.00	1997/06/13	8:43:14am
u40x0106m	6941	13 27 12.59	-47 29 53.29	F814W	100.00	1997/06/13	8:47:14am
u40x0107m	6941	13 27 08.22	-47 30 14.54	F300W	160.00	1997/06/13	9:48:14am
u40x0108m	6941	13 27 08.22	-47 30 14.54	F555W	100.00	1997/06/13	9:53:14am
u40x0109m	6941	13 27 08.22	-47 30 14.54	F814W	100.00	1997/06/13	9:57:14am
u40x010am	6941	13 27 08.19	-47 30 14.69	F300W	160.00	1997/06/13	10:03:14am
u40x010bm	6941	13 27 08.19	-47 30 14.69	F555W	100.00	1997/06/13	10:08:14am
u40x010cm	6941	13 27 08.19	-47 30 14.69	F814W	100.00	1997/06/13	10:12:14am
u40x010dm	6941	13 27 14.73	-47 30 37.77	F300W	160.00	1997/06/13	10:18:14am
u40x010em	6941	13 27 14.73	-47 30 37.77	F555W	100.00	1997/06/13	10:23:14am
u40x010fm	6941	13 27 14.73	-47 30 37.77	F814W	100.00	1997/06/13	10:27:14am
u40x010gm	6941	13 27 14.75	-47 30 38.09	F300W	160.00	1997/06/13	11:25:14am
u40x010hm	6941	13 27 14.75	-47 30 38.09	F555W	100.00	1997/06/13	11:30:14am
u40x010im	6941	13 27 14.75	-47 30 38.09	F814W	100.00	1997/06/13	11:34:14am
u40x010jm	6941	13 27 17.03	-47 29 31.73	F300W	160.00	1997/06/13	11:40:14am
u40x010km	6941	13 27 17.03	-47 29 31.73	F555W	100.00	1997/06/13	11:45:14am
u40x010lm	6941	13 27 17.03	-47 29 31.73	F814W	100.00	1997/06/13	11:49:14am
u40x010mm	6941	13 27 17.06	-47 29 31.58	F300W	160.00	1997/06/13	11:55:14am
u40x010nm	6941	13 27 17.06	-47 29 31.58	F555W	100.00	1997/06/13	12:00:14pm
u40x010om	6941	13 27 17.06	-47 29 31.58	F814W	100.00	1997/06/13	12:04:14pm
u40x010pm	6941	13 27 10.51	-47 29 08.51	F300W	160.00	1997/06/13	1:01:14pm
u40x010qm	6941	13 27 10.51	-47 29 08.51	F555W	100.00	1997/06/13	1:06:14pm
u40x010rm	6941	13 27 10.51	-47 29 08.51	F814W	100.00	1997/06/13	1:10:14pm
u40x010sm	6941	13 27 10.50	-47 29 08.19	F300W	160.00	1997/06/13	1:16:14pm
u40x010tm	6941	13 27 10.50	-47 29 08.19	F555W	100.00	1997/06/13	1:21:14pm
u40x010um	6941	13 27 10.50	-47 29 08.19	F814W	100.00	1997/06/13	1:25:14pm
u40x010vm	6941	13 27 10.73	-47 30 02.31	F555W	100.00	1997/06/13	1:31:14pm

After processing through the standard WFPC2 pipeline, stars must be identified and their positions measured in each of the images. The first step is to generate a master list of approximately 12500 stars in the combined field, using the tasks **daofind** and **phot**, and cross-identifying the outputs for each field on the basis of the approximate coordinates produced by the task **metric**. We then measure the pixel position of each star in each image that includes it, for a total of about 78,000 position measurements - on average about 6.5 per star. We measure the positions of each star both via centroiding and via Gaussian-fitting; neither method is ideal for undersampled data, and we estimate typical measurement errors of about 0.25 pixels. We adopt the Gaussian-fitting as slightly more stable. We determine approximate shifts and rotations on the basis of sigma-clipped coordinate differences, and identify (and reject) a small number of outliers - position measurements that deviate more than 3 pixels with respect to the Holtzman solution with the approximate image shifts. The resulting database of pixel positions is the input to the subsequent analysis.

Mathematical formulation of the problem

In our analysis, we treat the true positions of the stars on the sky as unknown but constant throughout the observing run. The geometric distortion is the solution of an optimization problem: we seek the transformations $T : (x_1, x_2) \rightarrow (y_1, y_2)$ from measured pixel positions (x_1, x_2) into a common system of coordinates (y_1, y_2) such that each star has the same final coordinate each time it is observed. The transformations T are composed of two parts: the rectification $R : (x_1, x_2) \rightarrow (z_1, z_2)$, which transforms the measured pixel positions (x_1, x_2) into a system of rectilinear coordinates (z_1, z_2) anchored to the camera's field of view, and a rototranslation $S : (x_1, x_2) \rightarrow (y_1, y_2)$, which accounts for the different pointing of the telescope for each observation, and consists of an offset and a rotation for each observation. The rectification R is different for each detector, but is assumed to be the same for all observations, although there are indications that the plate scale might change as a function of time, perhaps due to velocity aberration. The rototranslation is different for each observation, but it only causes a rigid motion of the relative positions of stars.

Of course, the transformed coordinates for each star will not be exactly the same in all observations, because of measurement errors, imperfections in the transformation, and so forth; therefore we seek to minimize the overall discrepancies in the least-squares sense. Formally, we define for each star i the average transformed position $(Y_1, Y_2)_i$ as:

$$(Y_1, Y_2)_i = \left(\sum_k (y_1, y_2)_{ik} \right) / N_i$$

where k for each star i runs over the N_i observations which include that star, and minimize the total quadratic error in the transformation:

$$Q = \sum_i \sum_k [(y_{1,ik} - Y_{1,i})^2 + (y_{2,ik} - Y_{2,i})^2]$$

where the sum is again over all stars i and all observations k containing that star.

The optimization involves the parameters that describe the rectification as well as the three parameters for each rototranslation. As indicated above, some of these parameters - namely the linear components of the transformation for one detector and the position and orientation for one of the images - remain unconstrained by the optimization. Where appropriate, we assume the same parameters as in the Holtzman transformation.

For the rectification R we assume the same functional form as in the Holtzman transformation. Specifically, we assume that (z_1, z_2) are expressed by complete third-order polynomials in (x_1, x_2) , in the form:

$$\begin{aligned} z_1 &= C_1 + C_2 \tilde{x}_1 + C_3 \tilde{x}_2 + C_4 \tilde{x}_1^2 + C_5 \tilde{x}_1 \tilde{x}_2 + C_6 \tilde{x}_2^2 + C_7 \tilde{x}_1^3 + C_8 \tilde{x}_1^2 \tilde{x}_2 + C_9 \tilde{x}_1 \tilde{x}_2^2 + C_{10} \tilde{x}_2^3 \\ z_2 &= D_1 + D_2 \tilde{x}_1 + D_3 \tilde{x}_2 + D_4 \tilde{x}_1^2 + D_5 \tilde{x}_1 \tilde{x}_2 + D_6 \tilde{x}_2^2 + D_7 \tilde{x}_1^3 + D_8 \tilde{x}_1^2 \tilde{x}_2 + D_9 \tilde{x}_1 \tilde{x}_2^2 + D_{10} \tilde{x}_2^3 \end{aligned}$$

where $\tilde{x}_1 = (x_1 - 400)$, $\tilde{x}_2 = (x_2 - 400)$. The form of the solution and the nomenclature $C_1, \dots, C_{10}, D_1, \dots, D_{10}$ for the coefficients are the same as in Holtzman et al (1995) and Trauger et al (1995). Of course, a different set of coefficients C, D , is defined for each detector. Also note that the (z_1, z_2) coordinate system is common to all four detectors; as in Holtzman et al (1995), we choose to align it approximately with the Planetary Camera.

The Holtzman and Trauger solutions revisited: rotation and translation of the detectors.

The first step is to verify whether the Holtzman and Trauger solutions provide an adequate model for the new astrometry data. However, we already know, both from science data and from the K-spot data discussed later, that the four WFPC2 detectors have moved with respect to each other since the geometric solutions were first derived, presumably as a consequence of physical changes in the WFPC2 optical bench. We thus modify both the Trauger and the Holtzman solution to allow for a solid-body motion - both translation and rotation - of each detector with respect to the reference PC detector. Thus limited, the rectification solution becomes a simple rototranslation for each detector, with only 9 free parameters: x-shift, y-shift, and rotation for each of the WF chips. These coefficients are determined by a least-squares fit to the data collected in the 14 F555W exposures we consider. In addition to the 9 parameters describing the shift and rotation of the WF detectors with respect to the PC, we need also to solve for the 39 parameters that describe the orien-

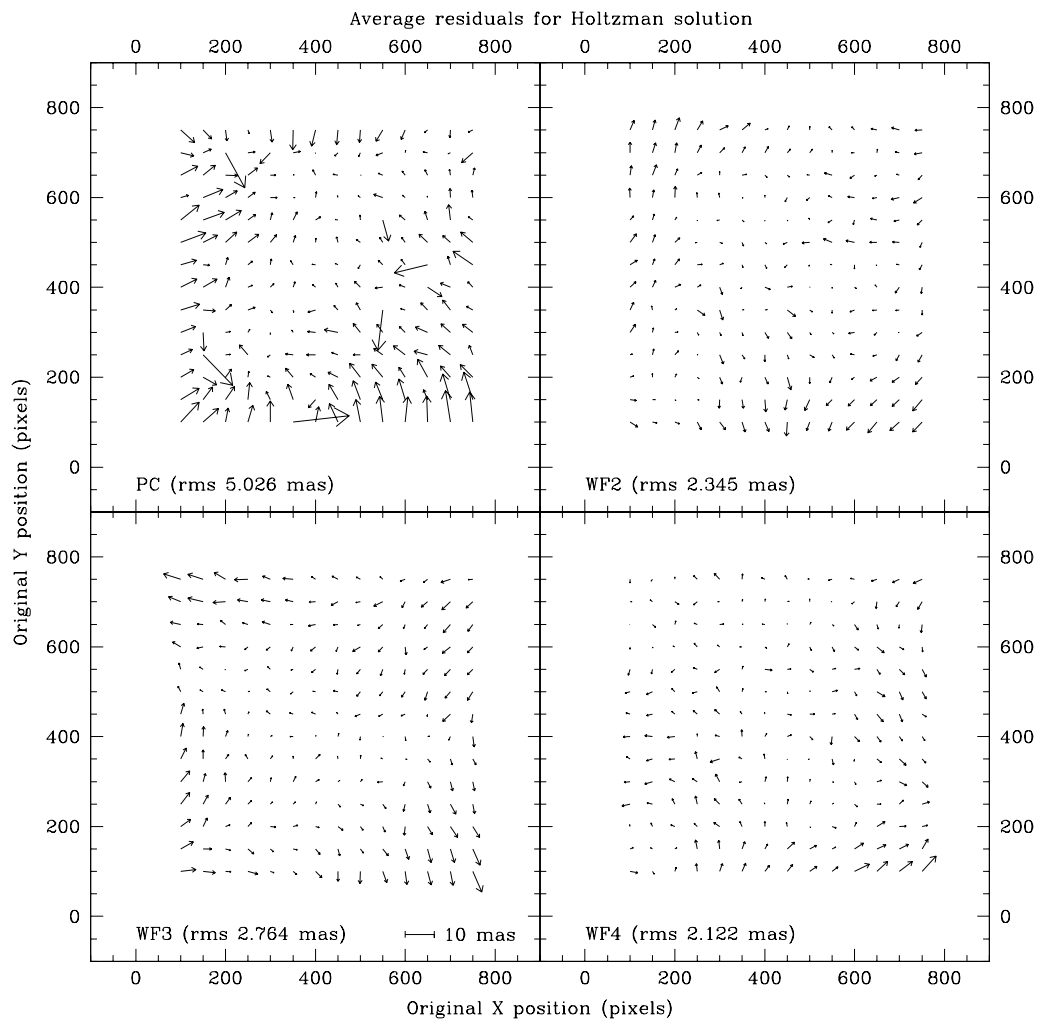
tation of each subsequent exposure with respect to the first; the total number of free parameters is thus 48. The new distortion coefficients resulting from this optimization are given in Table 2 for the Holtzman solution, and in Table 3 for the Trauger solution. In both cases, the rotation is consistent with zero, while a significant shift is measured for all three detectors.

The quality of each modified solution can be evaluated by plotting the residuals as a function of original pixel position. If the transformation is inaccurate in a certain region of the field of view, the transformed positions resulting from stars observed there will be systematically offset from their mean positions determined from their observations elsewhere in the field of view. Figures 2 and 3 show these residuals, averaged in 50x50 pixel regions over each of the WFPC2 detectors. The residuals are expressed in rectified pixels, of the same size as pixels at the center of the Planetary Camera, and scaled by a factor of 300, i.e., 300 units equal one PC pixel (46.65 mas); a scale bar and the rms of the residuals, averaged over each detector, are given in each Figure.

From Figures 2 and 3, it is apparent that the residuals for the empirical Holtzman solution are substantially smaller than for the Trauger solution. In fact, the Holtzman solution has fairly small residuals throughout the field of view, except in the corners of each camera where systematic residuals approach 10 mas (15 mas in the PC). The occasional large deviations in the PC are partly due to shot noise - the PC has a larger plate scale, and thus each 50x50 pixel box in Figures 2 and 3 contains typically one-sixth as many stars as the comparable box in each of the other detectors. However, there is also clear evidence for larger systematic residuals in the PC, presumably because the relatively sparse stellar field used for the Holtzman observations did not fully sample the PC aperture.

Table 2. Coefficients of the Holtzman solution, modified for detector shifts

#	C				D			
	PC	WF2	WF3	WF4	PC	WF2	WF3	WF4
1	3.543270e+2	-8.105789e+2	-8.047693e+2	7.721130e+2	3.436170e+2	7.684762e+2	-7.675412e+2	-7.715605e+2
2	1.000130e+0	19.361801e-3	-2.187390e+0	13.750306e-3	1.005350e-3	2.185891e+0	7.381839e-3	-2.186700e+0
3	0.979678e-3	-2.187871e+0	-8.491419e-3	2.188810e+0	0.999704e+0	20.044961e-3	-2.185360e+0	12.971496e-3
4	0.098414e-6	-1.509753e-6	-0.321418e-6	1.333156e-6	-0.580822e-6	-3.794486e-6	-1.498283e-6	1.308024e-6
5	-0.006313e-6	5.066731e-6	2.774332e-6	-4.007940e-6	-0.507180e-6	-2.994574e-6	2.966286e-6	2.017449e-6
6	-0.719924e-6	1.040543e-6	-2.068568e-6	-0.571239e-6	0.341546e-6	0.105853e-6	-0.202759e-6	-0.847583e-6
7	-37.389100e-9	-0.449795e-9	73.916314e-9	-2.004660e-9	-1.080820e-9	-74.779532e-9	-1.456379e-9	77.034510e-9
8	0.665047e-9	75.018818e-9	-1.188962e-9	-78.660908e-9	-34.204200e-9	-1.671252e-9	77.235689e-9	-1.684632e-9
9	-35.144100e-9	-1.511086e-9	77.299192e-9	-3.374268e-9	1.178100e-9	-75.524107e-9	0.853296e-9	77.519316e-9
10	-2.549830e-9	73.450779e-9	-0.373668e-9	-78.142602e-9	-44.892900e-9	0.307722e-9	76.795996e-9	-0.368805e-9

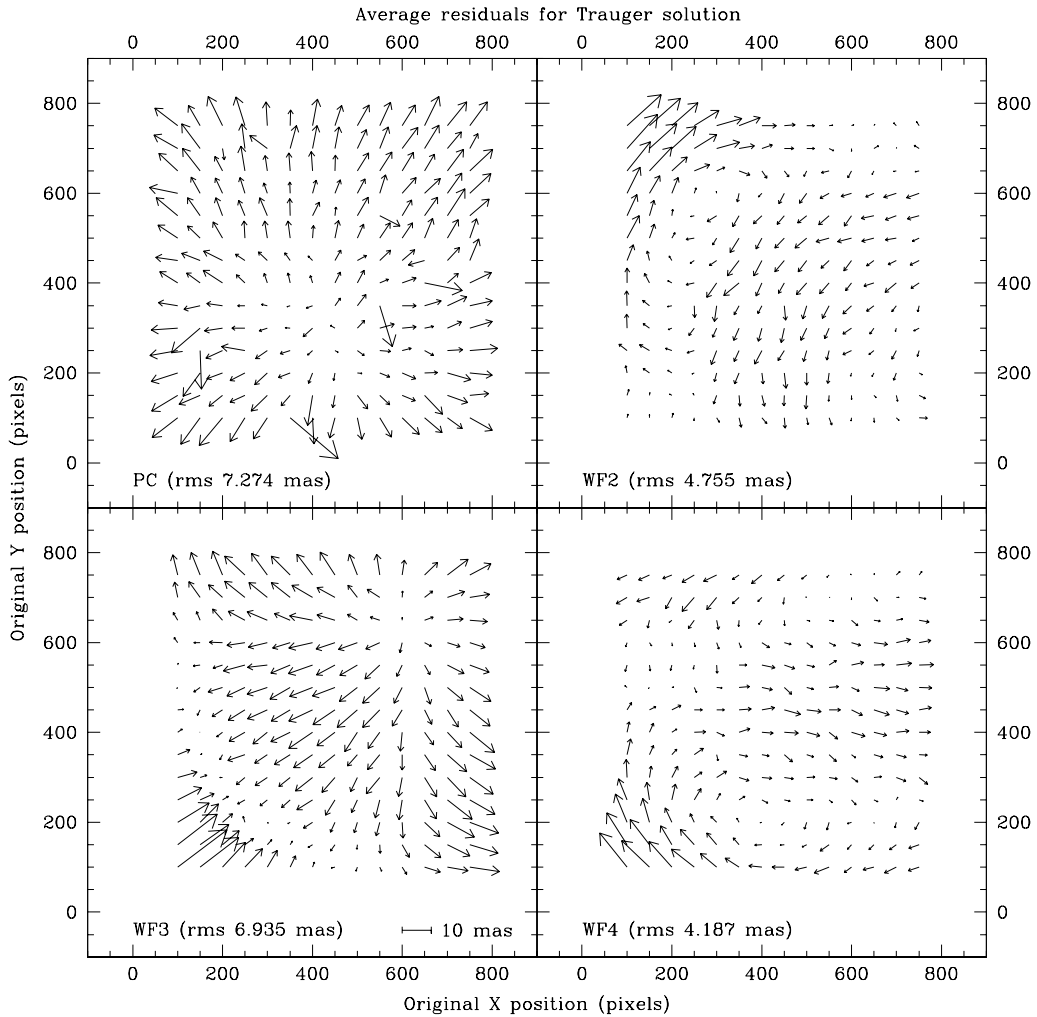
Figure 2: Zonal residuals for the modified Holtzman solution

On the other hand, the Trauger solution shows obvious systematics in all four cameras, with magnitude up to 20 mas. This difference may be partly due to the smaller number of independent parameters in the solution - many of the rectification coefficients vanish or are equal by construction, as can be seen for the PC in Table 2. (The rectification coefficients for the other cameras have the same symmetries, but these are not apparent in Table 2 because of the additional linear transformation needed to bring the coefficients into a coordinate frame aligned with the PC.) On the other hand, it must be emphasized that the Trauger solution is based purely on a priori calculations, and its success in describing the WFPC2 distortions without the benefit of any tunable parameters is impressive. The Trauger solution has also the substantial advantage of predicting the wavelength dependence of the geometric distortion, while the Holtzman solution is only valid for the F555W filter.

Table 3. Coefficients of the Trauger solution, modified for detector shifts, at 555 nm

#	C				D			
	PC	WF2	WF3	WF4	PC	WF2	WF3	WF4
1	3.543270e+2	-8.096135e+2	-8.039021e+2	7.717848e+2	3.436170e+2	7.685622e+2	-7.675659e+2	-7.717821e+2
2	0.999995e+0	19.300344e-3	-2.185197e+0	13.565845e-3	0.866987e-3	2.185784e+0	7.641823e-3	-2.186704e+0
3	0.866987e-3	-2.185773e+0	-8.772147e-3	2.186711e+0	0.999995e+0	20.430969e-3	-2.185193e+0	12.434739e-3
4	-1.070877e-6	-0.999889e-6	2.579879e-6	0.961447e-6	-0.913062e-6	-2.575361e-6	-0.985845e-6	2.591141e-6
5	-0.181943e-6	3.621248e-6	3.667208e-6	-3.677751e-6	-0.181943e-6	-3.687675e-6	3.639765e-6	3.634280e-6
6	-0.913062e-6	2.593109e-6	-0.966439e-6	-2.579527e-6	-1.070877e-6	0.952915e-6	2.587211e-6	-0.992188e-6
7	-35.062393e-9	-0.678571e-9	74.641872e-9	-0.444064e-9	0.000000e-9	-74.661802e-9	-0.280334e-9	74.693549e-9
8	0.000000e-9	74.728700e-9	0.280585e-9	-74.760475e-9	-35.104283e-9	-0.679179e-9	74.708752e-9	-0.444462e-9
9	-35.104283e-9	-0.679179e-9	74.708752e-9	-0.444462e-9	0.000000e-9	-74.728700e-9	-0.280585e-9	74.760475e-9
10	0.000000e-9	74.661802e-9	0.280334e-9	-74.693549e-9	-35.062393e-9	-0.678571e-9	74.641872e-9	-0.444064e-9

Figure 3: Zonal residuals from the modified Trauger solution, evaluated at 550 nm.



A new astrometric solution

Although the Holtzman solution, modified for the motion of the detectors, provides a good description of the geometric distortion in WFPC2, significant residuals remain at the level of 5 mas overall, and 10-15 mas in the corners of each detector. The Holtzman solution was based on a relatively sparse field, so that the detector corners could not be sampled very well, and it assumed perfect knowledge of the telescope motions between pointings. The observations obtained for Program 6941 were designed to obtain a very good sampling in all regions of the field of view, and thus allow for a better characterization of the solution. Therefore we attempted to obtain an entirely new solution driven entirely by the new data.

In order to take optimal advantage of the data, the method we use for the solution does not make any assumptions on external parameters - such as the motions of the telescope - but it simply attempts to optimize the consistency of the transformation, thus minimizing zonal residuals such as those shown in Figures 2 and 3. As discussed above, some of the parameters - primarily the linear terms in the solution for the PC - cannot be constrained with the available data; those parameters were left fixed at the Holtzman values.

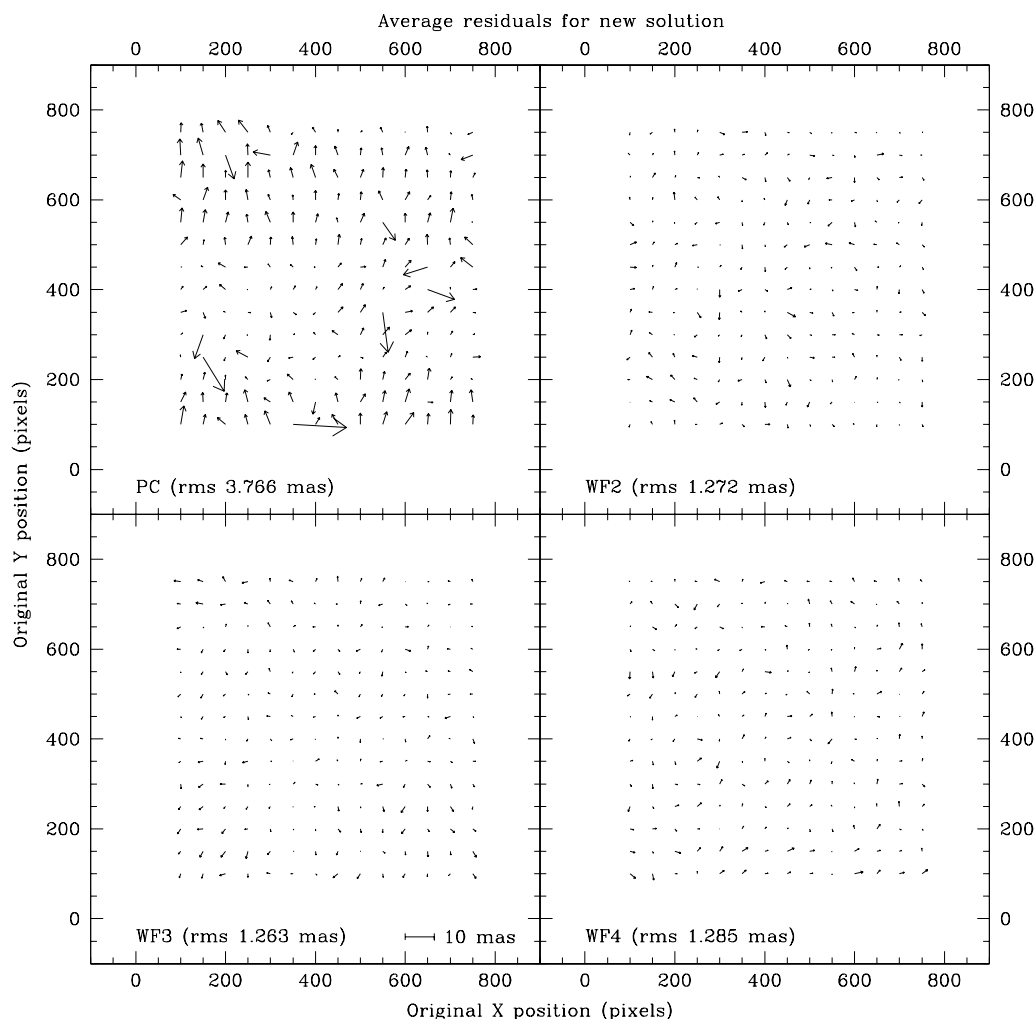
Table 4. Parameters of the new astrometric solution

#	C				D			
	PC	WF2	WF3	WF4	PC	WF2	WF3	WF4
1	3.543560e+2	-8.096405e+2	-8.052758e+2	7.708965e+2	3.436460e+2	7.667990e+2	-7.692243e+2	-7.708547e+2
2	1.000210e+0	21.667040e-3	-2.186307e+0	11.503445e-3	2.649830e-3	2.185899e+0	4.282145e-3	-2.186289e+0
3	1.685097e-3	-2.186781e+0	-10.318882e-3	2.187646e+0	0.999790e+0	16.771070e-3	-2.185173e+0	16.304679e-3
4	-0.476421e-6	-1.081274e-6	-0.467968e-6	1.410633e-6	-0.915545e-6	-3.953135e-6	-1.588401e-6	1.692025e-6
5	-0.128977e-6	4.875708e-6	2.360098e-6	-3.662324e-6	-0.347576e-6	-2.815106e-6	2.574760e-6	2.596669e-6
6	-1.119461e-6	1.160592e-6	-1.881792e-6	-0.820634e-6	0.532097e-6	0.309766e-6	0.404571e-6	-1.059466e-6
7	-38.989762e-9	-1.068123e-9	73.972588e-9	-0.388185e-9	-2.592636e-9	-73.394946e-9	-0.208263e-9	75.750980e-9
8	0.495226e-9	75.463250e-9	0.110498e-9	-77.222274e-9	-34.967762e-9	-1.715681e-9	77.114768e-9	0.528052e-9
9	-36.277270e-9	0.099408e-9	76.882580e-9	-1.794536e-9	-1.570711e-9	-75.104144e-9	0.162718e-9	75.946626e-9
10	-0.075298e-9	72.628997e-9	0.003372e-9	-76.141940e-9	-41.901809e-9	-0.423891e-9	74.483675e-9	-0.237788e-9

The resulting solution has the same form as the Holtzman solution, with the parameters reported in Table 3. The zonal residuals, computed exactly as for the modified Holtzman and Trauger solutions, are shown in Figure 4. It is immediately apparent that the systematic residuals are very small, especially in the WF cameras, where the systematic component is barely perceptible on the scale of the Figure. The rms residuals are about 1.2 mas in the WF cameras, and under 4 mas in the PC. There is some indication of a systematic pattern with a peak amplitude of 3 mas in the PC residuals, although the larger residuals appear to be primarily due to noise. The new solution thus provides a bet-

ter description of the geometric distortion in WFPC2 than either the Trauger or the Holtzman solution.

Figure 4: Zonal residuals of the new third-degree polynomial solution



The accuracy of the new solution is limited by several factors: the quality of the individual measurements of stellar positions, which can be greatly improved using, for example, the techniques of Anderson and King (2000); the accuracy with which the distortion can be reproduced by a third-degree polynomial; and possible image-to-image variations such as those in the plate scale found by Gilliland et al (2000).

However, substantial improvements in the static determination of the distortion solution may be of limited practical use, since any solution thus obtained will only be valid for a specific date and filter. The relative motion of the detectors continues at a rate of about 10 mas/year, resulting in larger variations over a few months than any residual systematics in the solution; the K-spot data (see next Section) also suggest that the noise in the relative position of the detectors at any given time is less than 5 mas, with occasional large deviations of up to 200 mas. The wavelength dependence has been predicted successfully by

Trauger et al (1995; see for example Barstow et al. 2001). However, their functional description requires that each of the distortion coefficients be described as a separate quadratic function of the refraction index of MgF₂ (the material of the lenses in front of each WFPC2 detector). They do not provide an analytic way of generalizing the coefficients measured at 555 nm to other wavelengths; and, since the index of refraction only varies substantially in the far UV, high-quality data at wavelengths shorter than 250 nm are needed in order to obtain useful constraints on the variation of the distortion coefficients as a function of wavelength. We indicate in the concluding remarks a possible way to overcome these difficulties and produce an improved time- and filter-dependent solution.

Table 5. Approximate x and y positions of K-spots

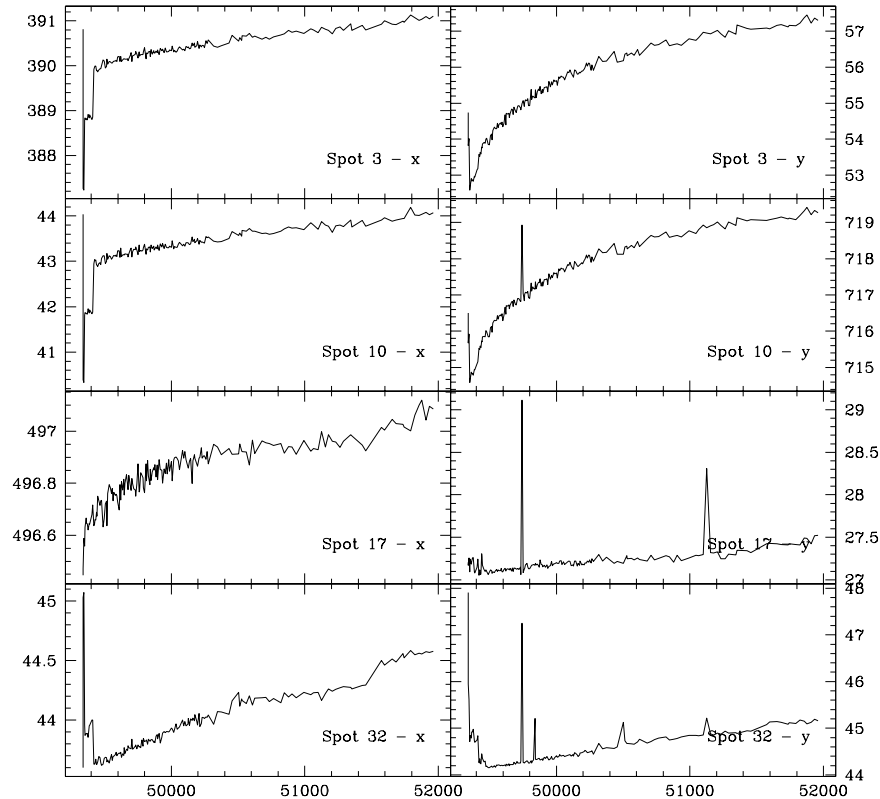
	PC			WF2			WF3			WF4		
	#	x	y	#	x	y	#	x	y	#	x	y
Pyramid edge parallel to x axis	1	75	54	11	63	23	32	44	50	54	54	42
	2	234	55	12	137	25	33	115.	44	55	131	43
	3	391	55	13	207	25	34	192	51	56	202	44
	4	550	55	14	281	27	35	262	49	57	273	46
	5	708	54	15	343	26	36	335	46	58	345	43
				16	427	28	37	407	50	59	421	40
				17	497	27	38	478	46	60	490	38
				18	570	28	39	547	39	61	563	43
				19	642	28	40	623	49	62	636	43
				20	715	28	41	697	50	63	708	41
Pyramid edge parallel to y axis	6	44	84	21	49	38	42	34	60	64	47	60
	7	45	243	22	48	111	43	37	134	65	43	135
	8	46	400	23	49	184	44	34	206	66	46	207
	9	45	559	24	49	250	45	37	275	67	45	281
	10	45	717	25	48	326	46	37	349	68	50	353
				26	47	400	47	34	427	69	42	422
				27	53	468	48	35	498	70	51	500
				28	46	552	49	27	426	71	45	558
				29	42	613	50	32	565	72	44	638
				30	43	689	51	32	638	73	45	712
				31	42	763	52	28	716			
							53	29	788			

K-spots

A clear indication of the movement of the chips with respect to one another is given by the K-spot data. The Kelsall spots, or K-spots, are images on the detectors of pinpoints of light generated by a lamp placed behind the WFPC2 pyramid. At some locations along the edges of the pyramid, the reflective coating is thinner, permitting the lamp light to shine through. Since the pyramid is at a spherically aberrated focal plane, each spot will

be refocused on the detector, producing a sharp, albeit aberrated, image. These bright spots identify the location of the pyramid edge on the detectors - and thus the usable region of each detector. In addition, changes in their apparent position on each detector indicate motions in the optical train after the pyramid; such motions will cause an identical change in the position of a celestial source on the detector. We identify 73 separate K-spots, at the approximate locations indicated in Table 5.

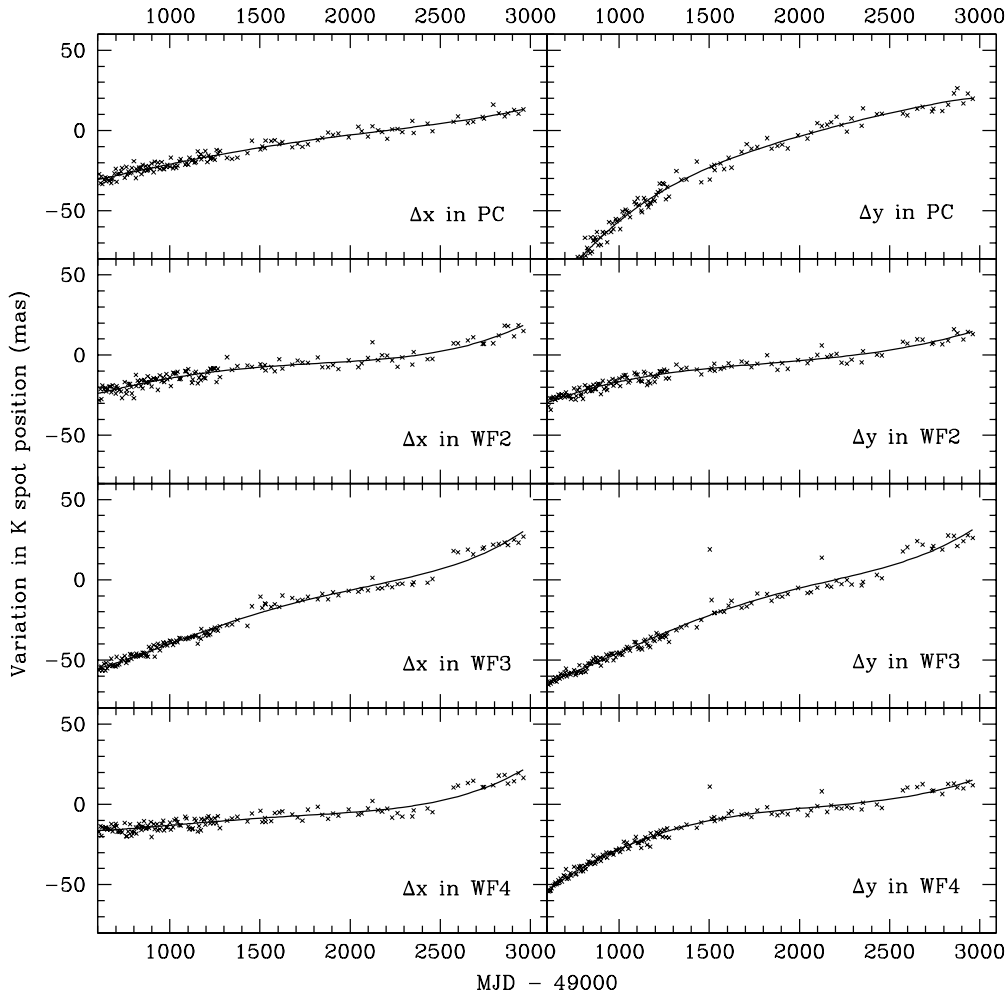
Figure 5: Time variation of the apparent position of selected K-spots, in detector pixels



We have determined the positions of the K-spots in 173 images taken throughout the life of WFPC2, approximately one every two weeks, representing about 20% of all K-spot images taken with WFPC2. At each epoch, we measure the pixel position of each of the K-spot images. We find that only 43 of the 73 K-spots in Table 5 yield useful position measurements; the images of the others are either extended or near other image artifacts, thus precluding a good quality measurement. The position of the spots varies regularly with time; Figure 5 shows a few examples. The position variation is highly systematic; with the exception of a few outliers, due to anomalies such as cosmic ray hits, all spot images within each chip move by the same amount, with a dispersion of about 0.1 pixels, thus indicating that the primary cause for the position variation is a lateral motion of the image with respect to the detector. Note that a rotation of the detectors would cause a dependence of the x motion on the y coordinate, and vice versa. Motions of other optical

elements would likewise cause distortions in the relative positions of the images. The motion was substantial during early on-orbit operation, amounting to 2-4 pixels over the first several months; this rapid shift is reflected in the Holtzman solution, which gives different values for the linear coefficients before and after March 4, 1994. Later on, the motion stabilized substantially, with an overall motion of about 0.1-0.2 pixel/year.

Figure 6: Average position of K spots in each detector and fourth-degree polynomial fit



If we neglect the early period of rapid and somewhat erratic motion, the relative position variation of the K-spots in each detector over time can be characterized by a simple polynomial fit, shown in Figure 6. The crosses represent the position shift (in mas) at each epoch for each detector, based on averaging the position changes of all usable K-spots in that detector, a 3-sigma clip was applied to eliminate outliers. The solid line is a fourth-

degree fit to the variation in each coordinate for each detector. Only points after MJD 49600 are shown. The coefficients given in Table 5 are for the expression:

$$dx, dy = A0 + A1 \cdot \tilde{t} + A2 \cdot \tilde{t}^2 + A3 \cdot \tilde{t}^3 + A4 \cdot \tilde{t}^4$$

$$\tilde{t} = (MJD - 50500)/1500$$

Almost all points fall within 5 mas of the polynomial fit, which can thus be taken to represent the relative motion of the detector over time. We should however note that the occasional larger deviations, of up to 150-200 mas, are real; the statistical uncertainty on each point in Figure 6 is approximately 2-3 mas.

Table 6. Coefficients of the fourth-order polynomial for the motion of WFPC2 detectors

Degree	x-PC	x-WF2	x-WF3	x-WF4	y-PC	y-WF2	y-WF3	y-WF4
A0	-10.74	-7.534	-20.58	-8.608	-23.01	-8.291	-22.17	-10.20
A1	26.98	13.74	50.8	11.31	72.68	16.75	61.29	34.41
A2	-11.23	-16.45	-27.78	-6.299	-60.68	-15.39	-33.08	-45.53
A3	2.558	18.13	-4.593	6.422	61.43	25.50	-9.375	32.33
A4	6.46	12.93	35.34	21.34	-29.83	-2.474	37.56	5.612

Suggestions for the future

The astrometric model for WFPC2 presented here, although improved, still falls short of what a WFPC2 observer may need. The most important element that remains missing from this empirical solution is the wavelength and time dependence. The K-spot data indicate a possible avenue for inclusion of the time dependence, via either estimated or measured variations in K-spot positions at a time close to that of the observation. However, it would be necessary to demonstrate how well the K-spot motions translate into changes in the astrometric solution for WFPC2. The wavelength dependence is predicted by the ray-tracing solution obtained by Trauger et al (1995); its major component appears to be a change in overall scale, rather than in the higher-order distortions. Therefore the wavelength dependence could be partially incorporated by including a wavelength-dependent plate-scale term in the solution. The tests required to validate both the wavelength and the time solution can probably be carried out with existing data, although regular verification may be needed. Finally, the accuracy of the position measurements on which the solution is based can be improved by using the Anderson and King (2000) method, perhaps obtaining sufficient information for a higher-order solution.

References

- Anderson, J., and King, I.R., 2000, *Toward High-Precision Astrometry with WFPC2. I. Deriving an Accurate Point-Spread Function*, PASP 112, 1360
- Barstow, M.A, Bond, H.E., Burleigh, M.R., and Holberg, J. B., 2001, Resolving Sirius-like binaries with the Hubble Space Telescope, MNRAS 322, 891
- Holtzman, J., et al, 1995, *The performance and calibration of WFPC2 on the Hubble Space Telescope*, PASP 107, 156
- Gilmozzi, R., Ewald, S., and Kinney, E. 1995, *The Geometric Distortion Correction for the WFPC Cameras*, WFPC2 Instrument Science Report 95-02
- Trauger, J.T., Vaughan, A.H., Evans, R.W., and Moody, D.C., 1995, *Geometry of the WFPC2 Focal Plane*, in *Calibrating Hubble Space Telescope: Post Servicing Mission*, A. Koratkar and C. Leitherer, editors (Baltimore: STScI), p. 379